

Evaluation of CT Techniques for Reducing Artifacts in the Presence of Metallic Orthopedic Implants

Douglas D. Robertson, Peter J. Weiss, Elliot K. Fishman, Donna Magid, and Peter S. Walker

Abstract: Metallic intramedullary orthopedic implants generate artifacts that can markedly degrade transaxial CT images. The artifacts, typically seen as starburst streaking, result primarily from reconstructions involving missing projection data. Two approaches are clinically available to reduce the artifacts around orthopedic implants. These are (a) the imaging of implants with lower attenuation coefficients or smaller path lengths (less attenuating objects) and (b) the planar reformatting of image data. The sizing accuracy of these two approaches was quantified using phantoms and the efficacy using cadaveric femoral specimens. Results demonstrated that metal artifacts may be reduced and accurate bony dimensional data obtained. **Index Terms:** Artifacts—Computed tomography, techniques—Bones, abnormalities—Prostheses.

Computed tomography has proved to be especially useful in evaluating musculoskeletal pathology. Unfortunately, standard transaxial CT images in the vicinity of metallic intramedullary orthopedic implants are badly degraded by artifacts. Left uncorrected, these artifacts make it difficult to determine the amount and quality of bone stock around implants. The artifacts, typically seen as starburst streaking, result primarily from image reconstructions involving missing projection data and also from partial volume effects, scatter, and aliasing (Fig. 1) (1-3).

Reduction of these metal-associated artifacts can be achieved in three ways. The simplest method, imaging less attenuating objects, involves avoiding or at least reducing the generation of the missing projection data. By using materials with lower X-ray attenuation coefficients (plastic \ll titanium $<$ stainless steel, cobalt-chrome) and implants with smaller cross-sectional areas (decreased metal path

lengths), it is possible to reduce the severe X-ray beam attenuations that produce the missing projection data. Increasing the effective X-ray energy can also be used to improve the beam penetration and reduce the missing projection data. However, this approach is limited by patient dose and by the requirement of a low effective energy for optimal bone mineral detection of the cancellous bone (4). The second method involves reformatting of the axial CT image data into interpolated new axial, orthogonal, or oblique images. Image reformatting into planes other than the scan plane will weight the true image signal over the pseudorandomly distributed artifactual signal when integrating between adjacent axial images. In this way the artifacts in the original axial images are averaged out of the planar reformatting. Commercially available software or services are available to perform multiplanar reformatting. The third and most sophisticated method of artifact reduction involves artificially generating values for the missing projection data and then reconstructing the image (5-8). Although work is in progress to produce this software, its use currently, even in the hands of skilled operators, requires too much time to be clinically feasible. This method was not tested for that reason.

This article reports on the results of an experimental study, using both phantoms and specimens, to assess the effectiveness of the two clinically

From the Orthopedic Biomechanics Laboratory, Brigham and Women's Hospital, and Harvard Medical School, Boston, MA (D. D. Robertson, P. J. Weiss, and P. S. Walker), and the Department of Radiology, Johns Hopkins Hospital, Baltimore, MD (E. K. Fishman and D. Magid). Address correspondence and reprint requests to Dr. D. D. Robertson at Orthopedic Biomechanics Laboratory, Brigham and Women's Hospital, 75 Francis Street, Boston, MA 02115, U.S.A.

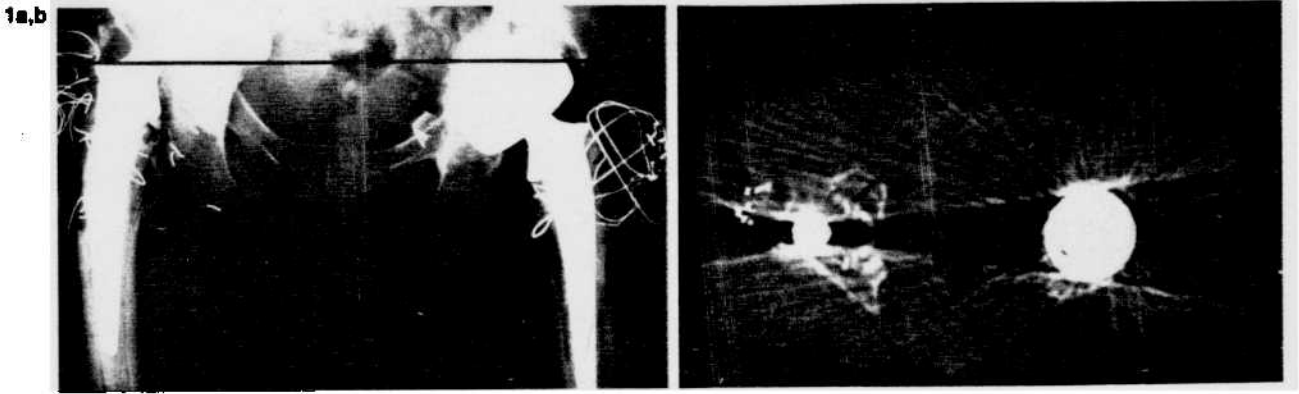


FIG. 1. An anteroposterior radiograph (a) illustrates the level at which the axial CT image (b) was taken in this patient with a right total hip replacement and a left bipolar femoral implant. Note the starburst streaking emanating from both prostheses.

available methods for reducing metal-associated artifacts, less attenuating objects, and planar reformatting. Intramedullary implants were used because they generate some of the worse metal-associated artifacts clinically encountered. Phantoms were used to quantify the accuracy of bone sizing around intramedullary implants and together with the cadaveric femoral specimens were used to demonstrate the qualitative effectiveness of these reduction artifact methods.

MATERIALS AND METHODS

The stem-bone phantoms were precision machined with dimensional tolerances within 0.05 mm. Phantoms were made to simulate cemented and press-fit hip stems. Cortical bone equivalent and bone cement equivalent materials with X-ray attenuations similar to those of cortical bone and bone cement were used. Orthopedic grade titanium-6Al-4V alloy, cobalt-chrome alloy, and stainless steel were used for the intramedullary stem materials as they are the most frequent hip stem and intramedullary rod materials. Four sizes of bone shafts were produced using epoxy-based cortical

bone equivalent material (9). Their outer to inner cortical diameters were 50:42 mm, 50:28 mm, 32:18 mm, and 32:12 mm (Figs. 2 and 3). These dimensions are representative of the range of sizes of cortical bone around intramedullary implants associated with the adult elbow, shoulder, hip, and knee. Bone cement-equivalent sheaths (hollow cylinders with 3 mm thick walls) were machined out of polycarbonate for each of the four cortical shaft sections. The intramedullary cylindrical rods were machined out of titanium-6Al-4V alloy, cobalt-chrome alloy, and stainless steel. A rod of each material was made to press-fit into each of the cortical shafts and into each of the polycarbonate sheaths.

Stem-bone specimens were also produced. Two pairs of proximal femurs were obtained from formalin-fixed cadavers. Anteroposterior and lateral radiographs were taken to rule out unsuspected disease and to assist in implant sizing. One pair had titanium-6Al-4V alloy hip stems (Omnifit, Osteonics, Allendale, NJ, U.S.A.) inserted, one with cement and one without cement (press-fit). The second pair received identically sized implants made of

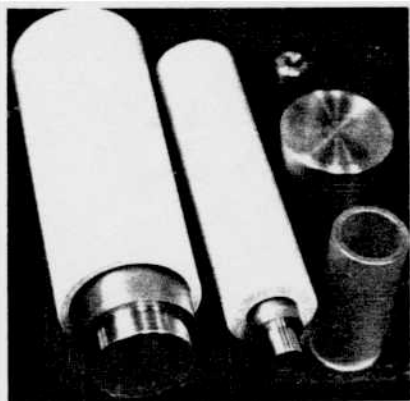


FIG. 2. Photograph of the stem-bone phantoms with their outer cortical cylinders, metal rods, and "cement" sheaths.

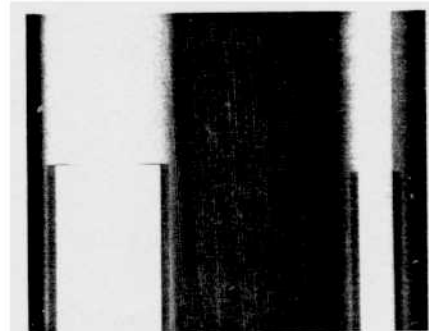


FIG. 3. Radiograph of the stem-bone phantoms. On the left is the 50 mm outer diameter section with a rod press-fit in the upper half and a "cemented" rod in the lower half. The "cement" (polycarbonate) sheath is seen as the lucent region between the rod and cortex. On the right is the 32 mm outer diameter section, also with a press-fit rod in the upper half and a "cemented" rod in the lower half.

cobalt-chrome. As with the titanium implants, the cobalt-chrome implants were also implanted, one with and one without cement.

The phantoms and specimens were individually aligned and placed in the center of a 17 cm diameter cylindrical water bath (approximately thigh-size). All CT studies were performed on a Somatom DR-3 scanner (Siemens Medical Systems, Inc., Iselin, NJ, U.S.A.) and reconstructed using the routine body kernel. Axial slices 2 mm thick were taken of the stem-bone phantoms, using two techniques: 125 kVp, 230 mAs, 3 s ("high") and 96 kVp, 300 mAs, 3 s ("low") energies. The two energy scans were obtained for each type of metal rod, with and without the plastic sheaths, for each of the four sized phantom sections. Following this, 10 contiguous 2 mm thick slices were obtained at each of the phantom sections at 125 kVp, 230 mAs, and 3 s. These contiguous axial scans were reconstructed using the Somatom's multiplanar reconstruction and display (MPR/D) software to produce planar images (1 pixel thick) orthogonal to the phantom's long axis (Fig. 4). The cadaveric specimens were scanned at 125 kVp, 230 mAs, and 3 s. A clinical protocol for multiplanar hip studies was followed and 4 mm thick slices were taken with 1 mm overlap along the length of the specimens. These images were also reformatted using the MPR/D software.

To evaluate sizing accuracy, the scanner's image processing software was used to measure the cross-sectional phantom dimensions (horizontal diameters) for all the axial and multiplanar images (Fig. 5). For the press-fit metal rods (no polycarbonate sheath), the outer bone phantom diameter and rod diameter were measured, respectively, at the full width at half maximum (FWHM) (10) for the interfaces of bone equivalent material and water and bone equivalent material and metal. For the "cemented" metal rods (with polycarbonate sheaths), the outer bone phantom diameter, inner bone phantom diameter, and rod diameter were measured respectively, at the FWHM for the interfaces of bone equivalent material and water, bone equivalent material and polycarbonate, and bone equivalent material and metal. Typical values, at

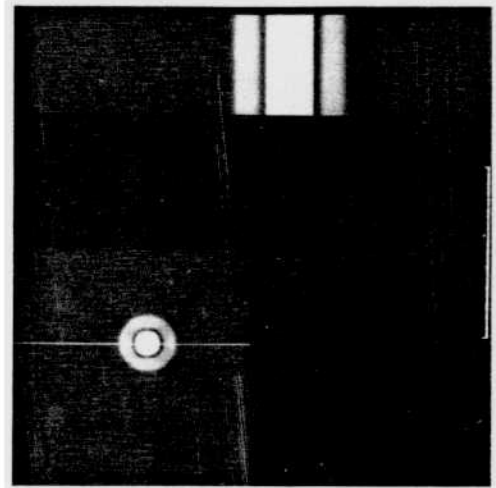


FIG. 4. Orthogonal image reformatting of the 12 mm cobalt-chrome rod within its "cement" sheath. Viewing settings are full width at half maximum for the interface of bone equivalent material and water. Bracket indicates 5 cm.

125 kVp, were 400 HU for polycarbonate, 1,300 HU for bone equivalent material, and 3,071 HU for metal. For each image the respective FWHMs were mathematically calculated from the image profile across the diameter of the phantom (horizontal diameter, parallel to the image's rows). At least two separate measurements of each material diameter were made off the CRT, by two of the authors, and the measurements averaged. The measurements were made using the Somatom's distance command. This was done by placing the cursor at the two ends of the line to be measured. A line angulation calculation was also made by the software and the angle of the line was always kept at zero. This helped to assure that the horizontal diameter was being measured. No sizing was performed on the 96 kVp images because most of the images were too noisy to reproducibly place the CRT cursor at the relevant interfaces (Fig. 6).

RESULTS

Measurement of the phantom dimensions from the transaxial and orthogonal images, in general,

5a,b

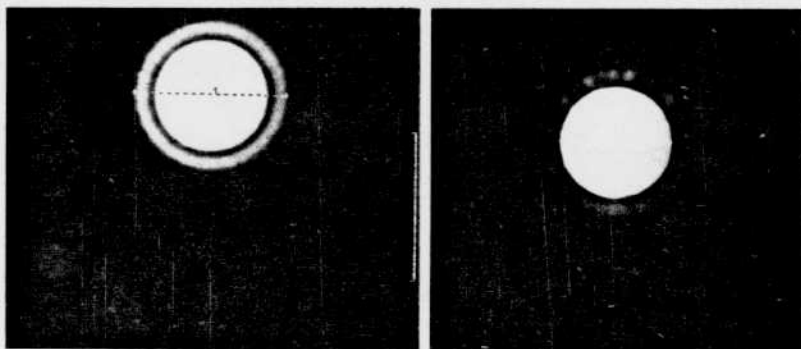


FIG. 5. Measurements of the outer bone phantom diameter (a) and the metal rod diameter (b) of the 50:42 mm phantom section. Brackets (right, a and b) indicate 5 cm. Viewing settings for measurements were at the full width at half maximum (FWHM) for the interface of bone equivalent material and water (a) and at the FWHM for the interface of bone equivalent material and metal (b).

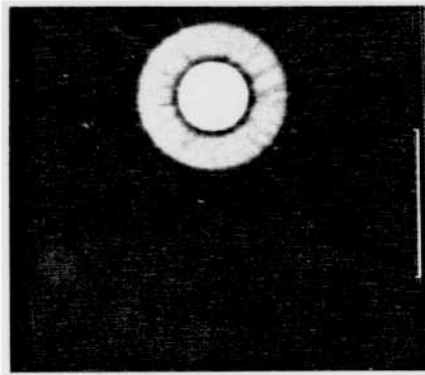


FIG. 6. Axial image, taken at "low" energy, of the phantom with the 22 mm diameter titanium rod in place. Viewing settings are full width at half maximum for the interface of bone equivalent material and water. Bracket indicates 5 cm.

agreed with the known physical dimensions (Table 1). The axial and orthogonal images of the phantoms were equally accurate (no significant difference, unpaired two-tailed *t* test). Multiplanar reformatting of the image data visually eliminated the artifacts if reconstructions were selected in planes that did not transect the artifact in the axial images. However, distance lines could also be passed through these areas in the axial images that were free of starburst artifact and measurements made. As neither the phantom geometry nor the phantom's relative position within the scanner changed along its length, image reformatting was not as visually dramatically different as with the specimens. The inner bone diameters around the 42 mm diameter press-fit stainless steel rod; the metal rod diameters around the 28, 36, and 42 mm stainless steel rods; and the metal rod diameters around the 28 and 42 mm diameter press-fit cobalt-chrome rods were not measured. As with the 96 kVp images the magnitude of the local artifact around the rods made it

difficult to reproducibly position the CRT cursor for the distance measurement. For all diameters of titanium alloy tested (6–42 mm), the average errors of outer cortical, inner cortical, and rod dimensions were all <5%.

Visual observations off the CRT of the axial and orthogonal images of the phantoms and specimens demonstrated that for equal cross sections the cobalt-chrome and stainless steel pieces had more streaking artifacts than the titanium pieces. Viewing settings were set at a conventional bone setting (220 center and a 2,300 window) and at the FWHM of the interface of bone and polycarbonate. The CRT images of the titanium pieces in general were artifact poor (artifact low enough to enable clear visualization of all the cross-sectional anatomy in the section) (Figs. 7 and 8). Orthogonal reformatting of the femoral specimens, with the cobalt-chrome and titanium implants, did improve the ability to visualize the surrounding cortical and cancellous bone. This was especially helpful proximally where the implant cross sections are the largest. Reformatting reduced the visually appreciable artifact content for the specimens because the implant's geometry and relative position changed along the length of the specimen.

DISCUSSION

Clinically, metal-associated artifacts may degrade image quality in the vicinity of surgical clips, dental fillings, heart valves, and orthopedic hardware (11–19). Artifacts from surgical clips and heart valves are primarily caused by motion, sharp edge effects, and aliasing. Artifacts around orthopedic hardware and dental fillings are caused primarily by the almost complete attenuation, in certain views, of the X-ray beam as it passes through the metal.

TABLE 1. CT measurement of the stem-bone phantom^a

	Actual phantom dimension	CT measured dimension around		
		Titanium rod	Cobalt-chrome rod	Stainless steel rod
Outer cortical diameter (mm)	50	50 (0)	50 (0)	50 (0)
	32	32 (0)	32 (0)	32 (0)
Inner cortical diameter (mm)	42	42 (0)	42 (0)	NM
(rod within cement sheaths)	28	28 (0)	28 (0)	28 (0)
	18	18 (0)	18 (0.6)	18 (0.6)
	12	12 (0)	12 (0.5)	12 (0.5)
Metal rod diameter (mm)	42	42 (0)	NM	NM
(rod press-fit)	36	36 (0)	37 (0.5)	NM
	28	28 (0)	NM	NM
	22	22 (0)	23 (0.5)	23 (0)
	18	18 (0)	19 (0)	19 (0)
	12	12 (0.5)	13 (0)	13 (0)
	6	6 (0.5)	7 (0.6)	7 (0.6)

^a Results of the four separate measurements are reported as the average (rounded to the nearest integer) and standard deviation (rounded to the nearest 10th) unless marked NM for not measured.

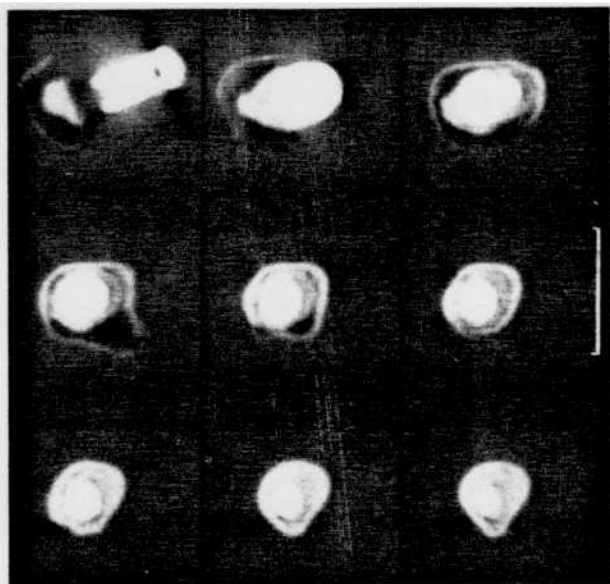


FIG. 7. Axial images through the cemented titanium implant. Viewing settings are full width at half maximum for the interface of bone and water. Bracket indicates 5 cm.

Just as the causes of artifacts around metal objects are different, so are their reductions. Surgical clip artifacts can be reduced by use of algorithms that remove projection data inconsistencies caused by the clip and replaces these inconsistencies with data consistent to that neighborhood (13). The imaging of clips made from less attenuating materials will also reduce clip artifact (11,16,17). Imaging less attenuating objects and image reformatting are two methods of reducing orthopedic implant-associated artifacts. Imaging less attenuating objects works by lessening or avoiding the primary cause of these artifacts. Image reformatting works because metal artifact in a given axial slice does not always align with artifacts in adjacent slices. This is due to changes in the geometry of the body and implant from slice to slice, as well as slice to slice changes in the positioning of the body and implant within the scanner. Thus some artifact can be averaged out by integrating between adjacent slices to create new axial, orthogonal, or oblique reformatting. Commercially available multiplanar reconstruction programs can easily be used to do this.

Our results demonstrate that CT can be used to obtain sizing information around some orthopedic implants. The magnitude of the error for single-energy X-ray CT sizing of cortical-bone and metal rod dimensions was initially surprising. It was expected that beam hardening, with smaller contributions from scatter and partial volume artifacts, would cause larger inner bone diameter errors (2,3,20). However, the results suggest that the bone-metal combination may have maximally hardened the X-ray beam, in this scanner configuration,

such that the expected inaccuracies were not seen. When measurable and wrong, the diameter measurements were off by 1 mm. This sizing error is approximately two times the pixel size but equal to the lower limit of measurement (1 mm) for the software used. Therefore, the rising percent error with decreasing metal rod diameters, in the face of a constant 1 mm absolute error, may be more a result of software limitations and the inability to reproducibly manually position the CRT cursor. Further investigations will use interpolation and curve fitting techniques to measure the dimensions with reproducibilities of at least a quarter of a pixel.

Computed tomography in certain situations may be used for evaluating structures around intramedullary orthopedic implants. Artifact-poor images can be obtained for routine CT images of orthopedic hardware made out of titanium or plastic or cobalt-chrome and stainless steel if they have small diameters (short material path lengths). Based on the work reported here, CT images of titanium hardware <36 mm in diameter and cobalt-chrome and stainless steel hardware <22 mm in diameter should be relatively artifact free. However as the material path lengths increase so will the artifact. Bilateral implants, with their large cumulative material path lengths in certain views, present the worst cases. Even when significant artifacts are present in the routine axial images it is still possible to reduce them by interpolating images, if the implant geometry or relative position of the implant in the scanner changes from slice to slice. Clinically useful images have been obtained using this approach (18,19).

The ability to obtain adequate anatomical infor-



FIG. 8. Orthogonal image reformatting (coronal) of the titanium cemented implant. Viewing settings are full width at half maximum for the interface of bone and water. Bracket indicates 5 cm.

mation around intramedullary orthopedic implants is critical to both pre- and postoperative assessments. We have used CT to detect avascular necrosis (in the contralateral side), which was not demonstrable by plain radiography. We have also used CT to assess the amount and location of cortical bone prior to revision total hip replacements. The presence of metallic intramedullary orthopedic implants in the region of interest should not be a contraindication to CT. In many instances CT may be used to provide accurate and clinically useful evaluations of skeletal pathology.

Acknowledgment: Special thanks are extended to C. Tymon for typing this manuscript and to B. Lasner for photographic assistance.

REFERENCES

- Hinderling R, Rügsegger P, Anliker M, Dietschi C. Computed tomography reconstruction from hollow projections: an application to *in vivo* evaluation of artificial hip joints. *J Comput Assist Tomogr* 1979;3:52-7.
- Joseph PM, Spital RD. The exponential edge-gradient effect in x-ray computed tomography. *Phys Med Biol* 1981;26:473-87.
- Joseph PM, Spital RD. The effects of scatter in x-ray computed tomography. *Med Phys* 1982;9:464-72.
- Müller A, Rügsegger P. Optimal CT settings for the evaluation of perimenopausal bone loss. *J Comput Assist Tomogr* 1985;9:607-8.
- Lewitt RM, Bates RHT. Image reconstruction from projections. III: Projection completion methods (theory). *Optik* 1978;50:189-204.
- Seitz P. Computertomographische osteodensitometrie beim metallischen kunstgelenk [Dissertation]. Zurich, Switzerland: Federal Institute of Technology, 1984.
- Seitz P, Rügsegger P. CT bone densitometry of the anchorage of artificial knee joints. *J Comput Assist Tomogr* 1985;9:621-2.
- Kalender WA, Hebel R, Ebersberger J. Reduction of CT artifacts caused by metallic implants. *Radiology* 1987;164:576-7.
- White DR, Martin RJ, Darlison R. Epoxy resin based tissue substitutes. *Br J Radiol* 1977;50:814-21.
- Baxter BS, Sorenson JA. Factors affecting the measurement of size and CT number in computed tomography. *Invest Radiol* 1981;16:337-41.
- Marks WM, Callen PW. Computed tomography in the evaluation of patients with surgical clips. *Surg Gynecol Obstet* 1980;151:557-8.
- Svendsen P, Quiding L, Landahl I. Blackout and other artefacts in computed tomography caused by fillings in teeth. *Neuroradiology* 1980;19:229-34.
- Glover GH, Pelc NJ. An algorithm for the reduction of metal clip artifacts in CT reconstructions. *Med Phys* 1981;8:799-807.
- Barneir E, Dubowitz B, Roffman M. Computed tomography in the assessment and planning of complicated total hip replacement. *Acta Orthop Scand* 1982;53:597-604.
- Cowan JC, Patrick D, Reid DS. Aortic root abscess complicating bacterial endocarditis demonstration by computed tomography. *Br Heart J* 1984;52:591-3.
- Weese JL, Rosenthal MS, Gould H. Avoidance of artifacts on computerized tomograms by selection of appropriate surgical clips. *Am J Surg* 1984;147:684-7.
- Gross SC, Kowalski JB, Lee SH, Terry B, Honickman SJ. Surgical ligation clip artifacts on CT scans. *Radiology* 1985;156:831-2.
- Fishman EK, Magid D, Robertson DD, Brooker AF, Weiss P, Siegelman SS. Metallic hip implants: CT with multiplanar reconstruction. *Radiology* 1986;160:675-81.
- Robertson DD, Fishman EK, Magid D, Weiss PJ, Kalender WA. Assessments of total hip replacements before and after revision surgery with use of computed tomography with metal-artifact reduction technique. *Radiology* 1986;161P:345.
- Robertson DD, Huang HK. Quantitative bone measurements using x-ray computed tomography with second-order correction. *Med Phys* 1986;13:474-9.